Analysis of Induced Color Index Error Due to Sequential Filter Photometry

Philip J. Castro
Applied Optimization Inc.
Tamara E. Payne, Luke W. Weisenbach
Applied Optimization Inc.
Trenton J. Godar, Veronica L. Wiley
U.S. Government
James Frith, Scott P. Milster
AFRL/RVSW

ABSTRACT

We present an analysis of induced color index error due to sequential filter photometry. We performed an analysis on multi-filter photometry signatures of three-axis stabilized Geosynchronous Earth Orbit (GEO) satellites to estimate the color index error due to forming color indices using sequential filter photometry. A color index is the difference in magnitude between two filters. Its formation assumes that the object's brightness is not changing during the collection of the two magnitudes.

For this analysis, we will utilize four-filter photometric signatures collected simultaneously. We performed glint season observations of GEO satellites using our system called Peacock with the goal of collecting simultaneous filter photometry that contains signatures that are rapidly changing. Peacock is a persistent, wide-field-of-view, simultaneous multispectral system built and operated by Applied Optimization.

The color indices formed from sequential filter photometry may contain non-negligible error when the object brightness is rapidly changing with respect to the filter duty cycle. We refer to this error as "induced color index error." Characterization of resident space objects using color indices could be affected by the induced color index error during these dynamic brightness periods. We converted the simultaneous signatures to form sequential signatures for our analysis. By forming color indices with the simultaneous data, which we define as truth, and taking the difference between color indices formed using the sequential data, we calculate the induced color index error. We found that the dynamic brightness regions due to solar panel glints and body glints of a three-axis stabilized GEO satellite signature contain induced color index error of up to about 30%. The Space Domain Awareness (SDA) community should be cognizant of the potential existence of this error when using color indices formed from sequential filter photometry for characterization, as this error is intrinsic and could not be reported by the SDA data providers.

1.0 INTRODUCTION

Sequential multi-spectral photometry has been used for decades by astronomers to study astronomical objects. The technique requires observing an object through spectral filters in a filter wheel cycling through each filter as quickly as possible. The filter duty cycle is the time it takes for the filter wheel to complete one cycle through all of the spectral filters. The duty cycle is a function of the exposure time required for good Signal-to-Noise Ratio (SNR), readout time of the sensor, and the time to cycle through the filters of the filter wheel. This technique has been used with great success by the authors and multiple others in the Space Domain Awareness (SDA) community for identification, characterization, and cross-tag detection/resolution for three-axis stabilized objects in Geosynchronous Earth Orbit (GEO) when observed from ground-based sensors [1] [2] [3] [4] [5]. This is because the viewing geometry of the GEO satellite from a ground-based sensor is not changing (three-axis stabilization) and the illumination angle is changing slowly with time (~ 15 degrees per hour) with respect to the filter duty cycle.

However, performing Space Object Characterization (SOC) using sequential filter photometry will have induced errors if these conditions are not met. Frequently, objects of interest (debris nearby an active satellite, a satellite losing attitude control, a satellite hit by debris, or even distinguishing between a rocket body and a satellite) will violate these conditions since their attitude could be changing faster than the filter duty cycle. If one part of the

satellite is observed through one filter and another part of the satellite is observed through another filter, then the color index formed by these two filters will not be representative of the satellite color. Even for three-axis stabilized GEO satellites during glint season, their brightnesses are so dynamic during the solar panel glints that the color index can be affected.

Therefore, SDA needs a more robust technique than sequential filter photometry for characterizing a wider array of objects and during any illumination condition. The solution is simultaneous filter photometry, where the intensity of the object is observed through all spectral filters at once. There are a few options for achieving simultaneous spectral filter photometry. One is to use a low-resolution grating or grism. Another is to use a beamsplitter in conjunction with spectral filters. Another is to use multiple telescopes, each with its own spectral filter and sensor. Applied Optimization (AO) chose the latter option, which maintains the optical throughput to maximize the SNR while keeping the aperture size and the cost small.

AO's system, Peacock[1], is used for persistent observations of GEO satellites. It has four telescopes mounted together and boresighted with image capture synchronization. Each telescope has a ~ 4-degree x 4-degree Field of View (FOV) with the Sloan filters, g', r', i', and z'. Four filters yield six independent color indices that are used in conjunction with clustering algorithms to characterize GEO satellites and to identify and then resolve cross-tags. Systematic errors in the color indices affect the efficacy of the SOC technique since it will induce confusion for the clustering algorithms.

Since the color index is an important measure for SOC and is also used in change detection algorithms, we seek to quantify how much error is induced with sequential photometry and under what conditions. We estimate the error in a color index introduced by sequential filter photometry for targets whose brightnesses are dynamic using simultaneous filter photometry as the benchmark for this paper.

2.0 METHODS AND PROCEDURES

Observations were performed in September and October 2021 to collect glint season data on Resident Space Objects (RSOs) using the Peacock system. Glint season photometry of RSOs is rapidly changing since the reflectance angles are coincident with the angles of observation obeying Snell's Law. These rapid changes in brightness allowed an analysis to determine empirically the induced error in the color index from sequential filter photometry. Observations were collected in four Sloan filters (g', r', i', and z') simultaneously on eight GEO satellites in a single FOV:

- Amazonas 2 (35942)
- Amazonas 3 (39078)
- Amazonas 5 (42934)
- Echostar 15 (36792)
- Echostar 16 (39008)
- Echostar 18 (41592)
- Telstar 14R (37602)
- Telstar 19V (43562)

The data were processed using AO's in-house processing pipeline that outputs Electro-Optical Space Situational Awareness (EOSSA) files with the simultaneous photometric results. The EOSSA files contained the required information to run ColorTool, which calculates the color index signatures needed for this analysis.

The images from all four sensors were simultaneous within microseconds. This simultaneity is important for this study since it ensures that the color index value calculated from simultaneous photometry is "truth," and that the difference between color indices calculated from simultaneous photometry and sequential photometry is the error solely induced by sequential spectral collections.

[1] See paper at this conference for more details on Peacock. Payne, et. al, "Peacock: A Persistent Wide-Field-Of-View Simultaneous Multispectral System Based on COTS Hardware", AMOS conference, 2022.

Differential photometry was performed using the APASS DR10 catalog. Since the night was photometric, this was performed on a single frame to estimate the mean difference between the instrumental magnitudes and the catalog magnitudes (zero-point prime) for g', r', i', and z' and applied to all of the frames for the night. This calibration process placed the instrumental magnitudes onto the Sloan photometric system.

We then converted the simultaneous photometry into sequential filter photometry using the following method. The collections with Peacock are simultaneous g'r'i'z' collections for 15-second exposures with a 4-second readout. Images are captured repeatedly for the entirety of the night from astronomical dusk to astronomical dawn. The algorithm that simulates sequential filter photometry from the simultaneous photometry uses the sequence of images taken in four adjacent exposures: g'r'i'z', g'r'i'z', g'r'i'z', and g'r'i'z'. We use the g'-band image from the first exposure, the r'-band image from the second exposure, the i'-band image from the third exposure, and the z'-band image from the fourth exposure to simulate sequential photometry in g'r'i'z'.

This process is then repeated for the entire night of observations. A night's worth of sequential four-filter photometry is used to form EOSSA files for each GEO satellite. Now we have two sets of observations in EOSSA (simultaneous and sequential) for each GEO satellite that can be compared and analyzed directly.

The simultaneous and sequential signatures were both run through ColorTool to calculate the color indices for all combinations of filter pairs. The color index is the magnitude in one filter subtracted from the magnitude in a second filter. Specifically, the g'- r' color index is defined as:

$$CI_{g'-r'} = g' - r' = m_{g'} - m_{r'} = -2.5 \log_{10} \frac{f_{g'}}{f_{r'}}, \text{ where the flux, } f_\lambda, \text{ is in units of } ergs\ cm^{-2} s^{-1} A^{-1}.$$

Since we are using real data, not every image in the g'r'i'z' sequence is always usable. Star contamination can sometimes occur. Therefore, we set a maximum for the timeframe that we will form a color index. This maximum time window was set differently for the simultaneous than for the sequential. For the simultaneous data, the time window was 1.0 second. The maximum time window for the sequential data was 4.0 minutes.

A time series of color indices forms color index signatures when the time is converted to longitudinal phase angle. We then compare the simultaneous color index signature to the sequential color index signature. Recall that since the simultaneous color index is considered "truth," the difference between these two signatures at each time step is the induced color index error solely due to the sequential collection of the data.

With an EOSSA file of simultaneous g'r'i'z' signatures and an EOSSA file of sequential g'r'i'z' signatures of the same satellite for the same night, we empirically determine the induced color index error. The induced color index error is defined as the difference in color indices between the two color index signatures. To calculate the difference between the two color index signatures, the simultaneous signatures are linearly interpolated so as to match the timing of the sequential color index signatures before the difference is calculated. This is necessary because the simultaneous color index data is of a higher cadence (resolution in time) compared to the sequential color index data.

3.0 RESULTS

First, we will highlight spectral signatures using Echostar 16 (39008) as an example. Then we will use three GEO satellites for the analysis of the color index errors: Telstar 14R (37602), Echostar 16 (39008), and Echostar 15 (36792). We will consider the color indices r'-i', and r'-z', and i'-z'.

The calibrated g'r'i'z' signatures of Echostar 16 (39008) for the night of September 28, 2021 (September 29, 2021 UTC) are shown in Fig. 1. The x-axis is the Longitudinal Phase Angle (LPA), and the y-axis is the exo-atmospheric magnitude. We used the APASS DR10 catalog for calibrations. We show the g'-band data, but there were issues causing drop-outs, so the g'-band data will not be used in the following color index error analysis.

There are several features in the signatures to note. The peak around -10 degrees LPA is the solar panel glint. The solar panel glint is partially obscured by the eclipse of the GEO satellite by the Earth, shown by the absence of data points from about -5 to 10 degrees in LPA. There is a small and sharp glint at about 60 degrees LPA and a broader

glint from about 60 to 75 degrees LPA. These glints are from the body since the solar panels are on edge and have minimal cross-sectional area pointed at the sensor at 60 degrees LPA. The g', r', and i' bands appear to have a much better SNR than the z' band, which shows more dispersion in the latter part of the signature. This could be due to the atmospheric seeing becoming worse throughout the night or a possible loss of focus.

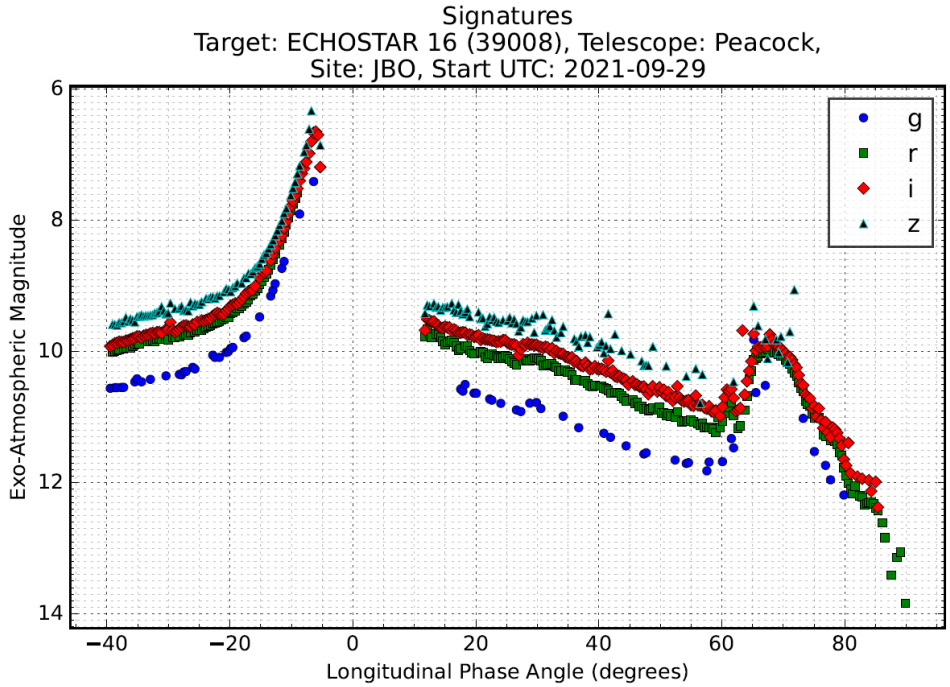

Fig. 1. Calibrated Peacock g'r'i'z' signatures of Echostar 16 (39008) for the night of September 28, 2021 (September 29, 2021 UTC)

The following figures comprise three-tiered plots. The top plot displays the spectral signatures in two spectral bands for both the simultaneous data and the simulated sequential data; the middle plot shows the color index signature formed from those two bands; and the bottom plot is the differences between the simultaneous and sequential color indices. These differences are the induced color index errors from the sequential photometry.

3.1 Telstar 14R Induced Color Index Errors

Fig. 2 shows the results for the r' and i' bands for Telstar 14R. The only glint feature in the signature is the solar panel. The induced color index errors were found to be as large as 0.20 magnitudes. The results for Telstar 14R with the r' and z' bands are shown in Fig. 3 where the induced color index errors are as large as 0.33 magnitudes. The results for Telstar 14R using the i' and z' bands are shown in Fig. 4. The induced color index errors are as large as 0.28 magnitude in this case. Note that in the observing sequence, r'i'z', that the largest time step between these three filters is r' and z', which shows the largest induced color index error from sequential observing.

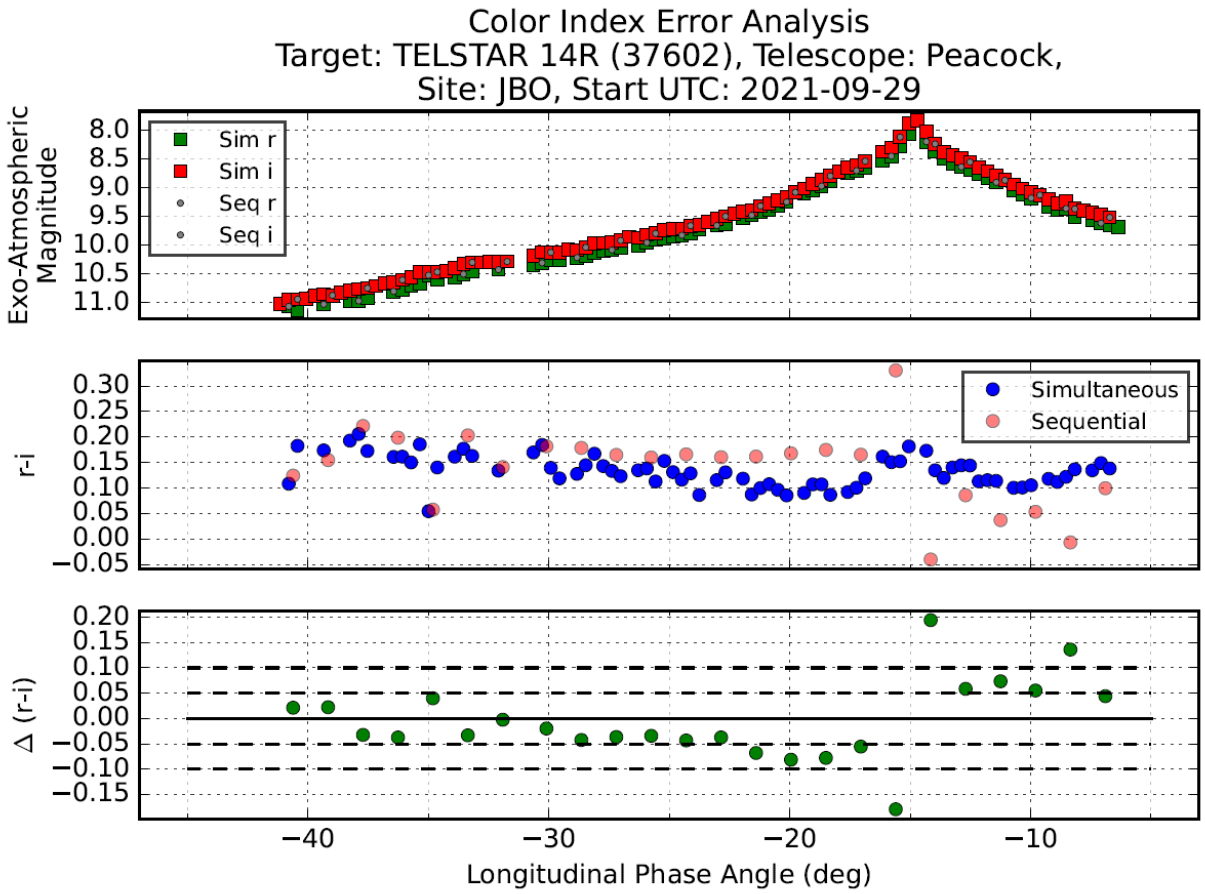

Fig. 2. Telstar 14R (37062) r' and i' simultaneous and sequential signatures (top), corresponding r'-i' color index signatures (middle), and induced color index error results (bottom)

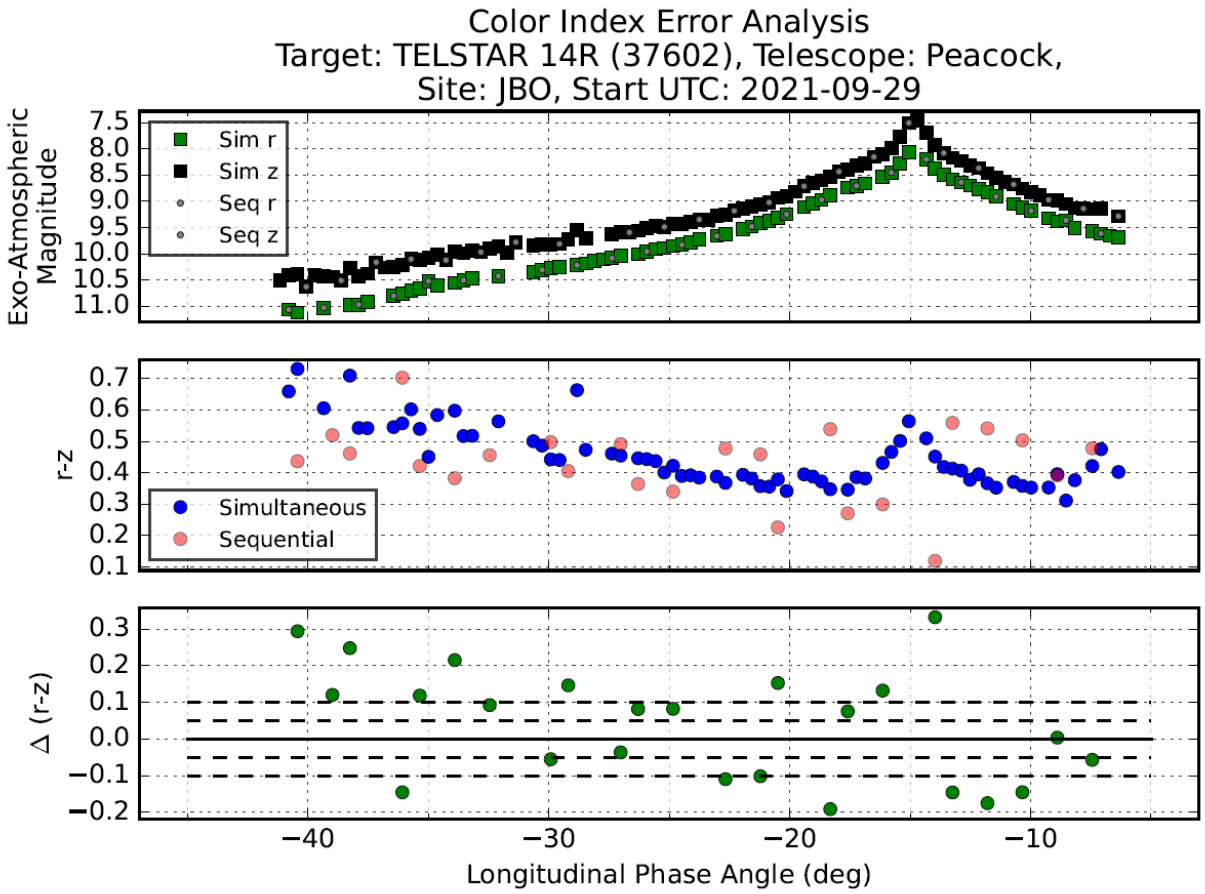

Fig. 3. Telstar 14R (37062) r' and z' simultaneous and sequential signatures (top), corresponding r'-z' color index signatures (middle), and induced color index error results (bottom)

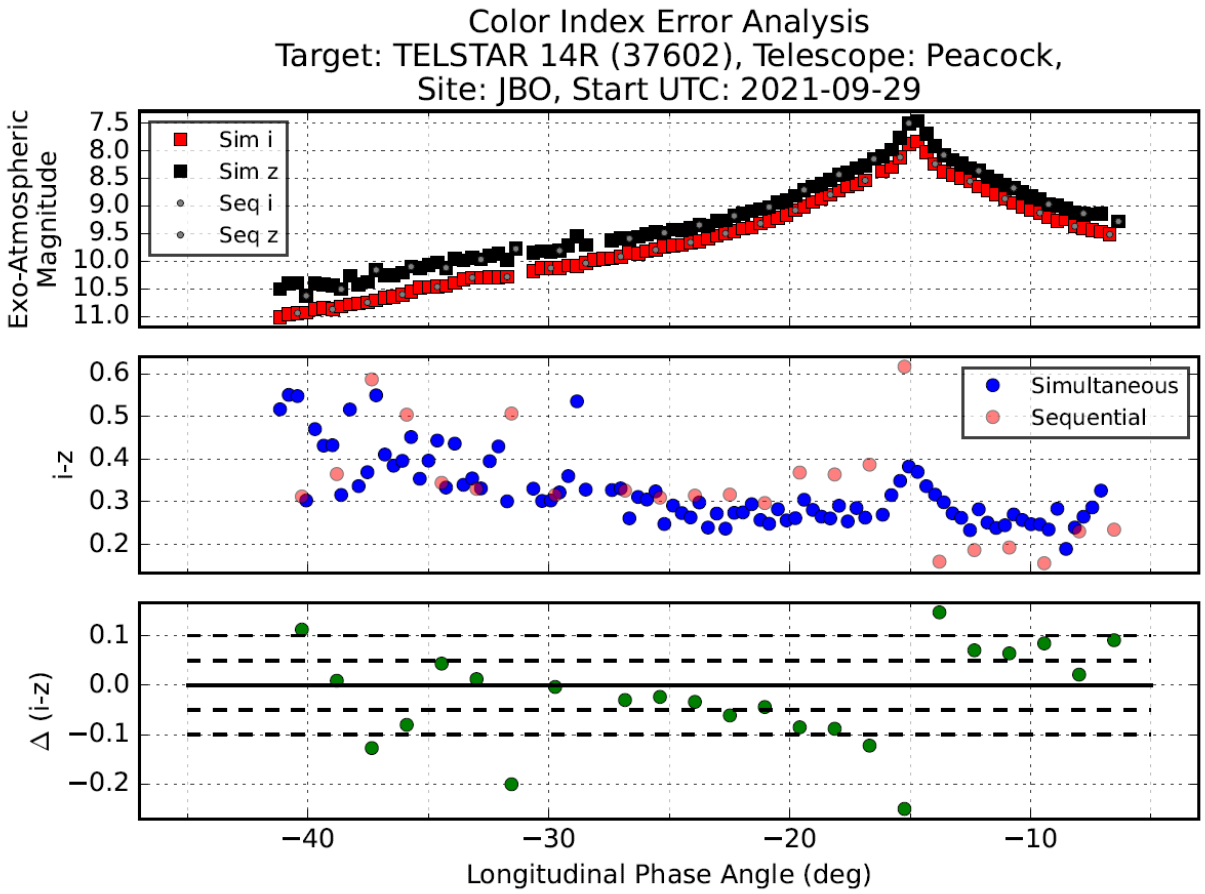

Fig. 4. Telstar 14R (37062) i' and z' simultaneous and sequential signatures (top), corresponding i'-z' color index signatures (middle), and induced color index error results (bottom)

3.2 Echostar 16 Induced Color Index Errors

Fig. 5 shows the results for the r' and i' bands for Echostar 16 for the solar panel glint. For the solar panel glint the induced color index errors can be as large as 0.11 magnitudes. Fig. 6 shows the body glint for the r' and i' bands, the induced color index errors are as large as +0.19 and -0.21 magnitudes. The body glint does not appear in the z' band. Therefore, the remaining results for Echostar 16 containing the z' band only show the solar panel glint. Fig. 7 shows the results for the r' and z' bands for the solar panel glint. For this color index, the induced color index errors are as large as 0.22 magnitudes. Fig. 8 shows the results for the i' and z' bands for the solar panel glint. The induced color index errors are as large as 0.18 magnitude in this case. Note that again the largest time step between these three filters (r' and z') resulted in the largest induced color index error.

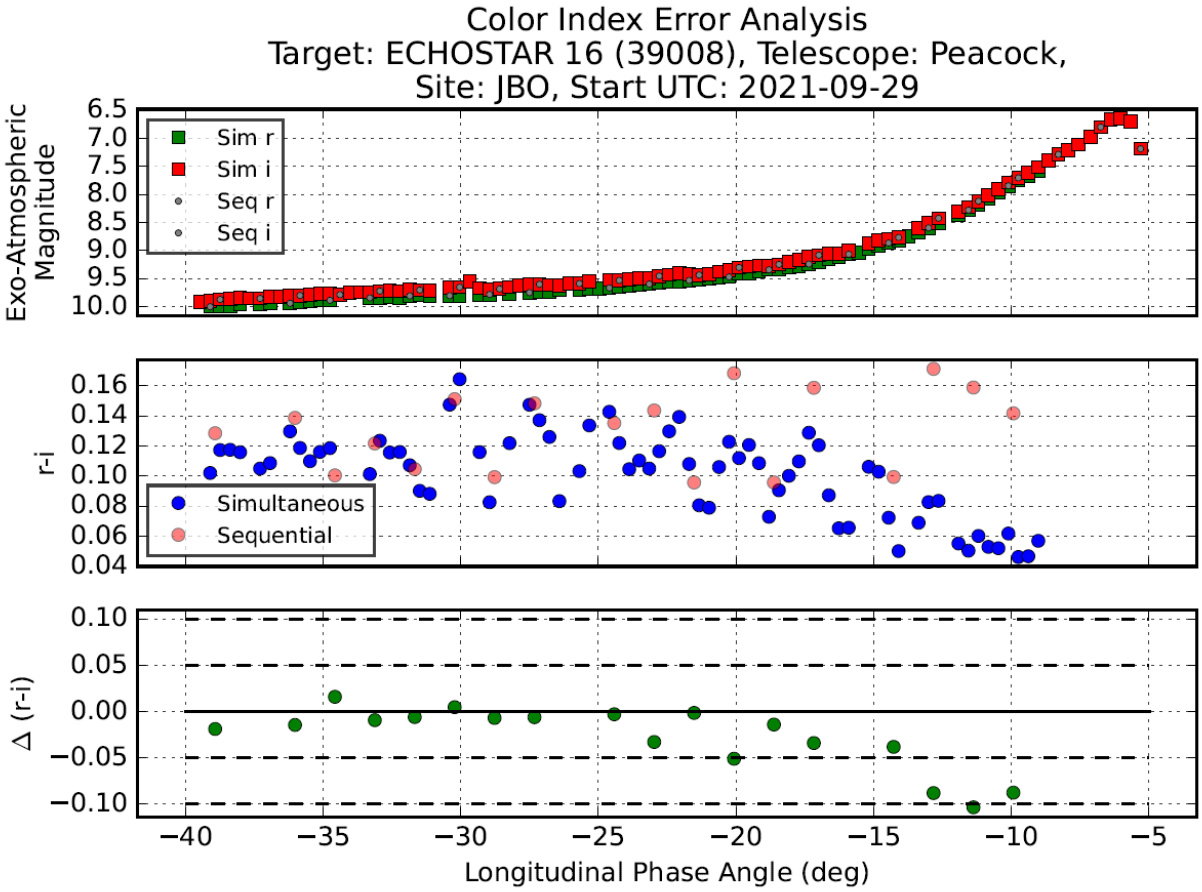

Fig. 5. Echostar 16 (39008) r' and i' simultaneous and sequential signatures of the solar panel glint (top), r'-i' color index signatures of the solar panel glint (middle), and induced color index error results for the solar panel glint (bottom)

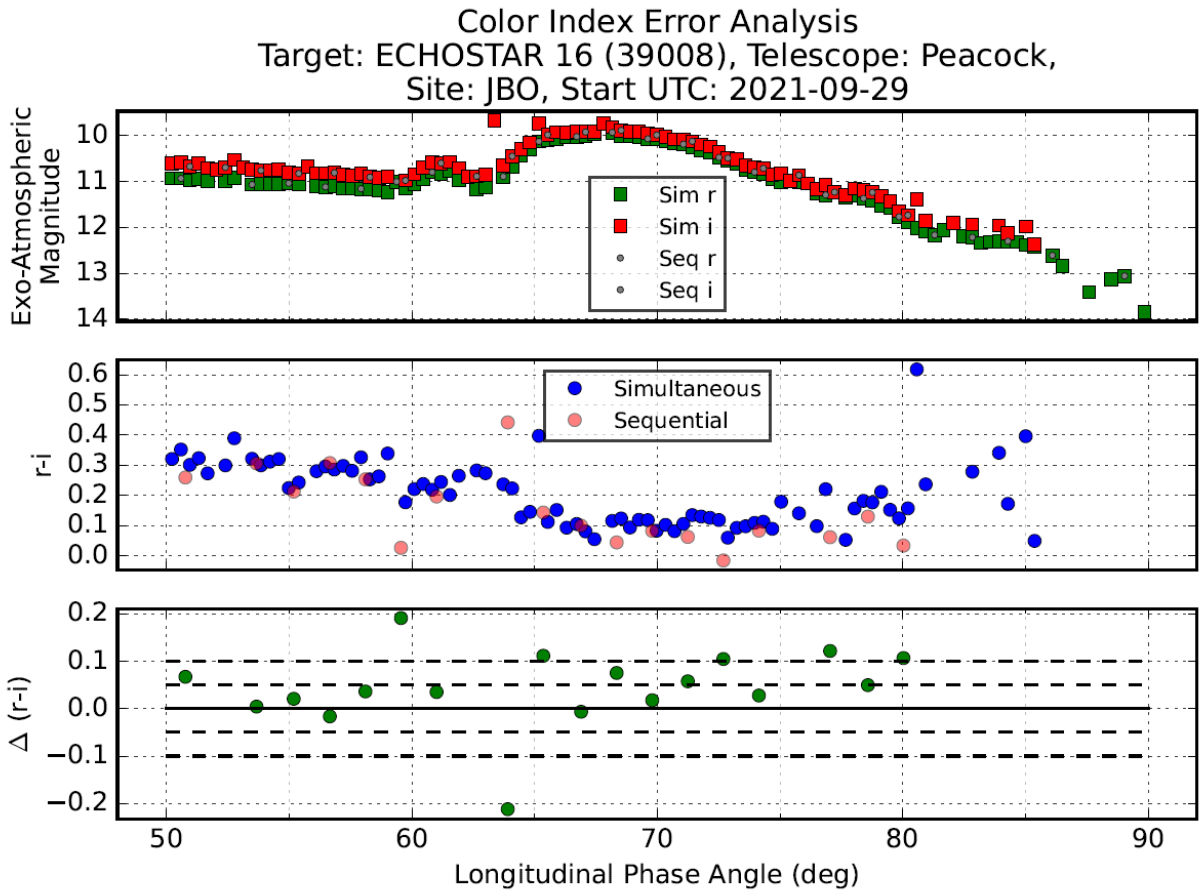

Fig. 6. Echostar 16 (39008) r' and i' simultaneous and sequential signatures of the body glint (top), r'-i' color index signatures of the body glint (middle), and induced color index error results for the body glint (bottom)

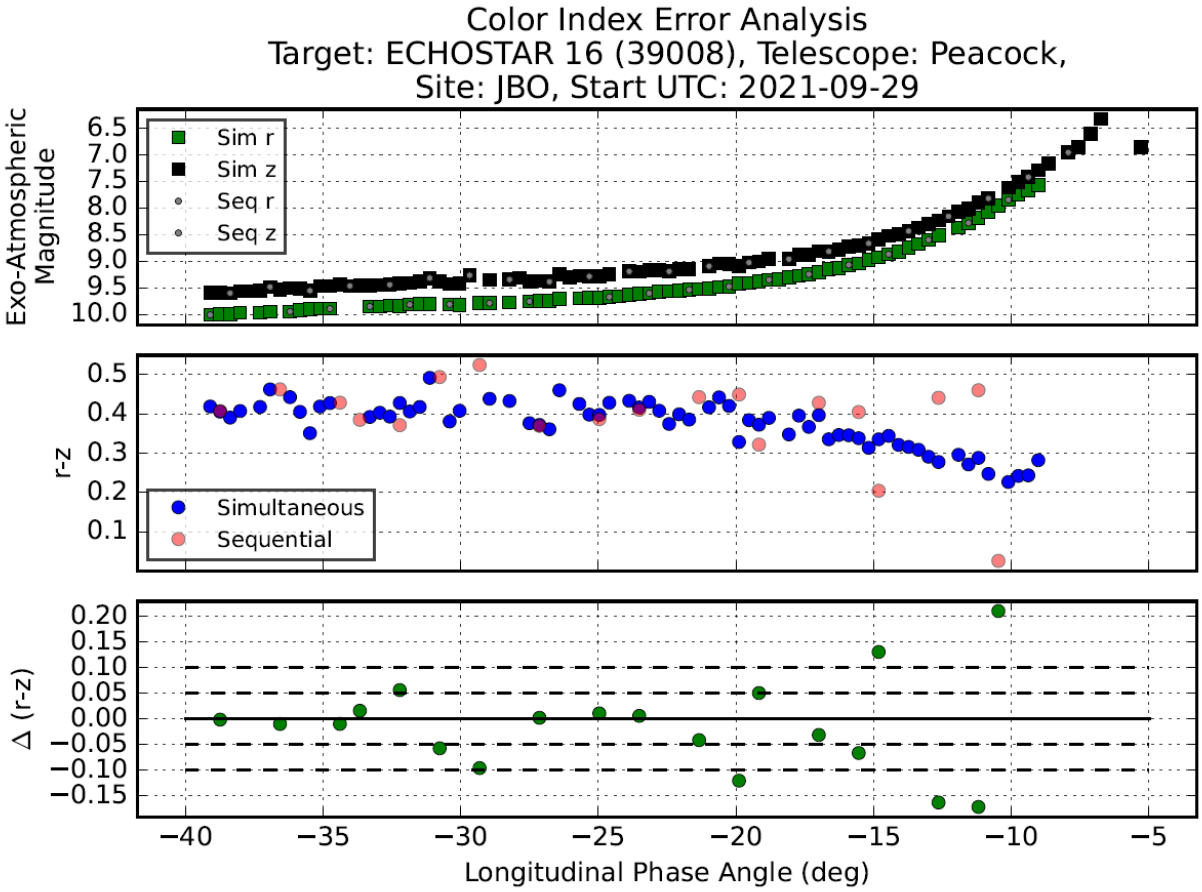

Fig. 7. Echostar 16 (39008) r' and z' simultaneous and sequential signatures of the solar panel glint (top), r'-z' color index signatures of the solar panel glint (middle), and induced color index error results for the solar panel glint (bottom)

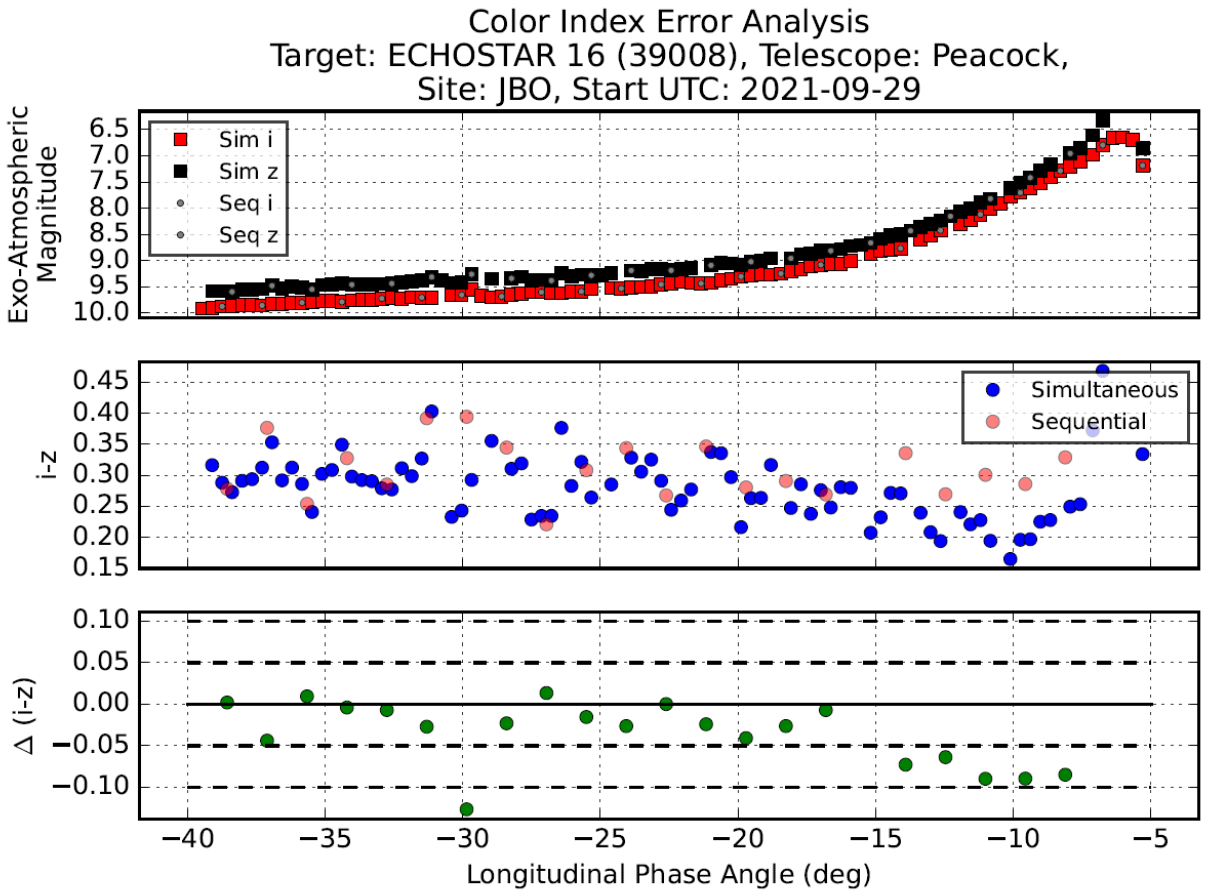

Fig. 8. Echostar 16 (39008) i' and z' simultaneous and sequential signatures of the solar panel glint (top), i'-z' color index signatures of the solar panel glint (middle), and induced color index error results for the solar panel glint (bottom)

3.3 Echostar 15 Induced Color Index Error

Echostar 15 exhibited only one major glint associated with the solar panel. Thus, in the following analysis, we only show the signature in the -40 to -5 degrees LPA range that captures the solar panel glint. Fig. 9 shows the results for Echostar 15 for the r' and i' bands capturing the solar panel glint. Note that the induced color index errors can be as large as 0.13 magnitudes. The results for Echostar 15 with the r' and z' bands in Fig. 10 shows the induced color index errors are as large as -0.24 magnitudes. Similarly for the i' and z' bands shown in Fig. 11, the induced color index errors are as large as -0.23 magnitude in this case. Note that the largest time step between these three filters (r' and z') resulted in only a slightly larger induced color index error in this case.

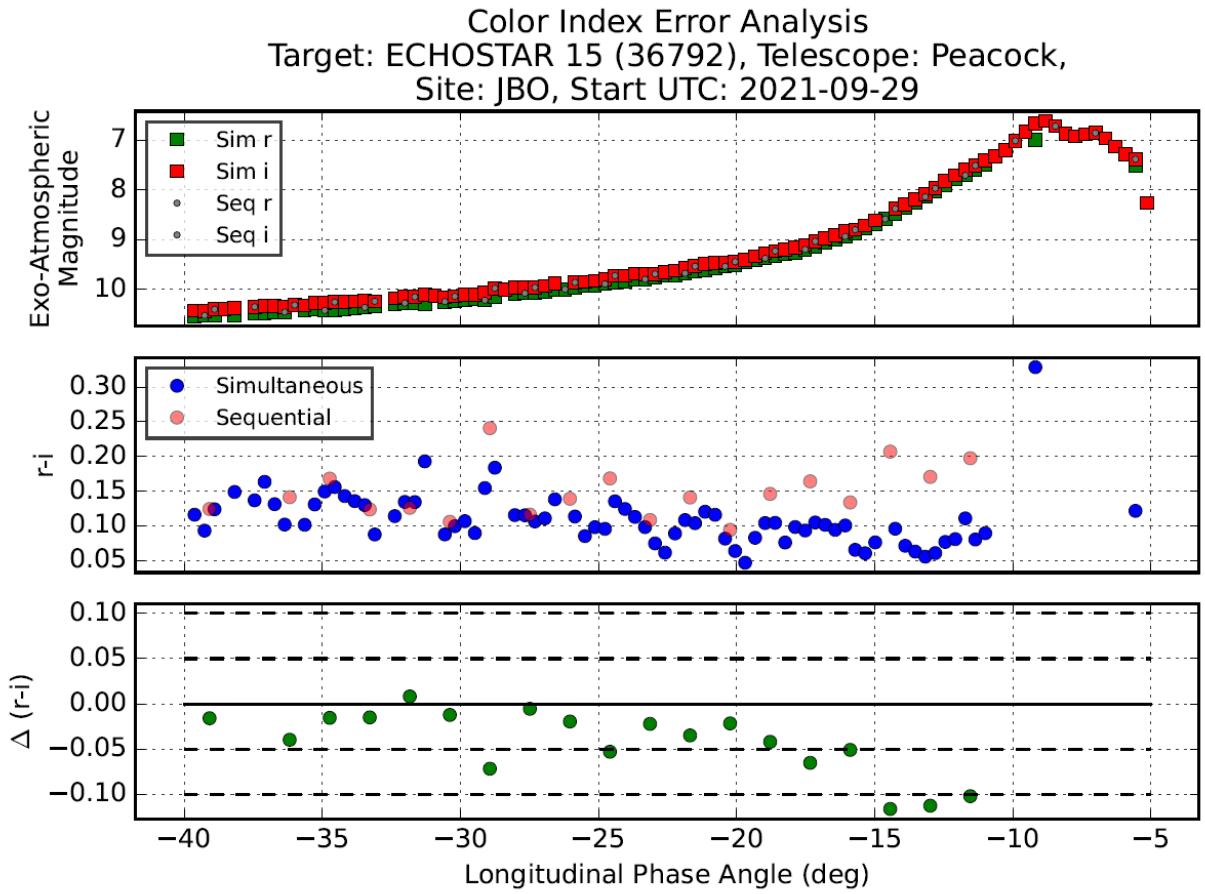

Fig. 9. Echostar 15 (36792) r' and i' simultaneous and sequential signatures (top), the r'-i' color index signatures (middle), and induced color index error results (bottom)

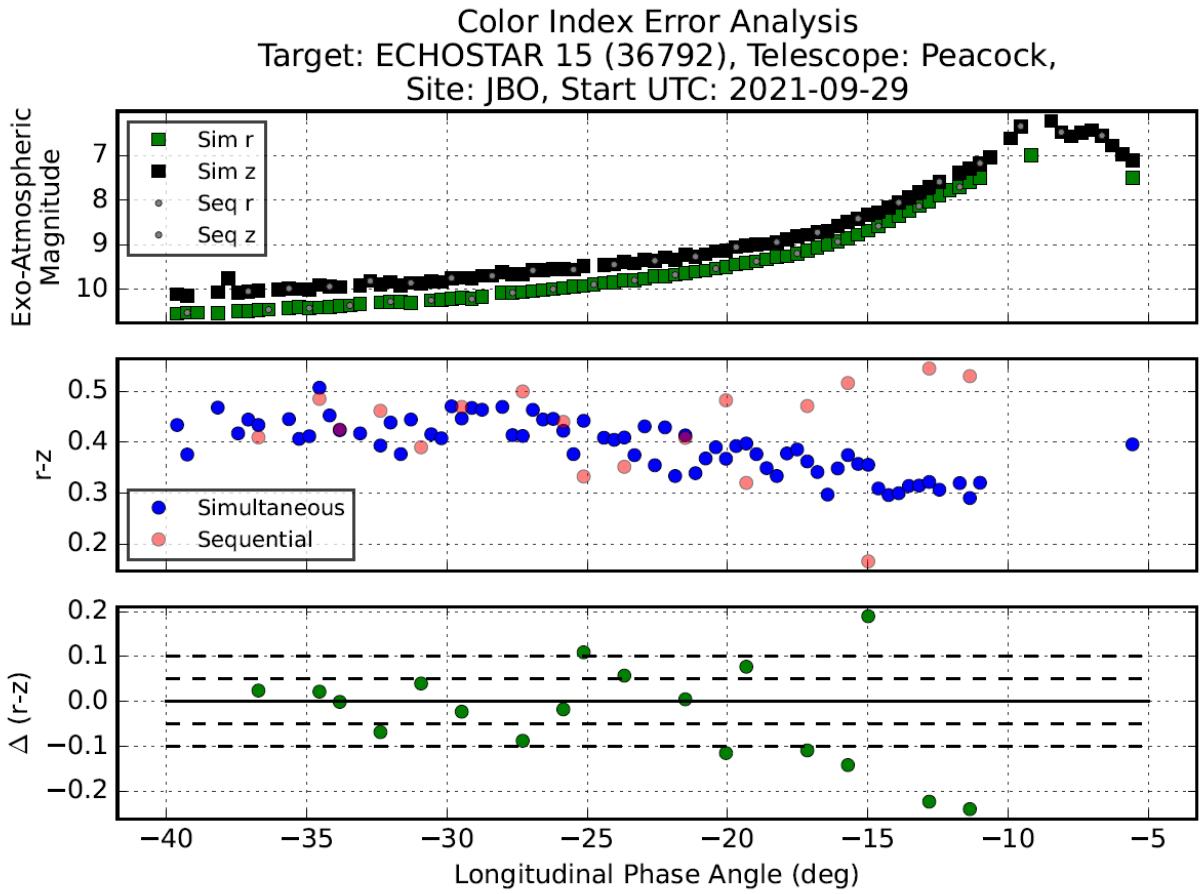

Fig. 10. Echostar 15 (36792) r' and z' simultaneous and sequential signatures (top), the r'-z' color index signatures (middle), and induced color index error results (bottom)

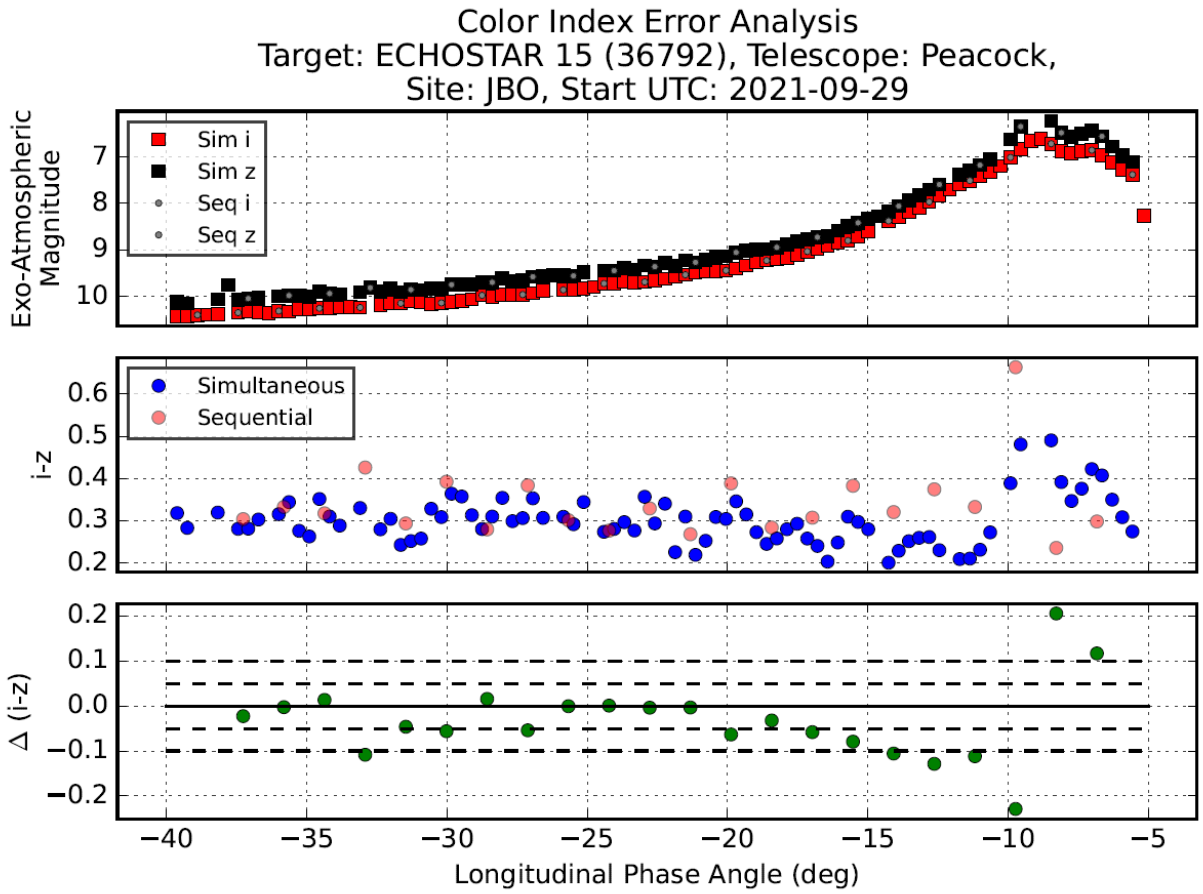

Fig. 11. Echostar 15 (36792) i' and z' simultaneous and sequential signatures (top), the i'-z' color index signatures (middle), and induced color index error results (bottom)

4.0 CONCLUSIONS

We demonstrated empirically the induced systematic error for color indices due to sequential filter photometry. The induced color index errors we found using three satellites ranged from **5 to 20%** with the largest error found to be **30%**.

For SOC, the color indices should have accuracies of around the 5-10% level or better. The induced color index error found in this study exceeds this level. The solar panel glint and the body glints are vital clues to characterizing a GEO satellite as a whole. The color characterization of each glint provides insight into the material composition of the respective components, playing a vital role in SOC. Although only three different targets were measured, over 25 years of empirical data collections by the authors have shown that the glints observed of these GEO satellites are typical of satellites over the Continental US (CONUS), the Pacific Ocean, and the Indian Ocean.

When performing characterization using sequential filter photometry rather than simultaneous filter photometry, caution must be taken to factor in the induced color index error. These errors are hidden and intrinsic and may result in the inability to properly perform characterization and discrimination on three-axis stabilized GEO satellites. For two-axis stabilized RSOs or tumbling RSOs that naturally exhibit frequent and extreme brightness changes orders of magnitude larger than shown in this analysis, sequential filter photometry is untenable to use for characterization and discrimination.

5.0 FUTURE WORK

Future work that would improve upon this analysis includes additional observations of RSOs and an alternative method to calculate color indices. Additional collections of GEO satellites during the glint season as well as non-glint season are desired. Observing a variety of GEO satellites during various times of glint season would allow a more thorough exploration of the rates of brightness change during this time of year for the GEO satellite population. Observations of GEO satellites during non-glint season would provide an in-depth exploration and analysis of body glints, since these may occur at any time of the year, and only one body glint was analyzed in this work.

Observations of other types of RSOs besides GEO satellites would explore RSOs that may exhibit larger rates of brightness change than GEO satellites. For example, low Earth orbit satellites have rapidly changing illumination conditions that may result in rates of brightness change larger than those associated with GEO satellites and therefore larger values of induced color index error than shown in this analysis.

The color index calculated here was performed by directly taking the difference between the magnitudes of two different filters. Future work would perform an additional analysis by calculating the color index using linear interpolation. It is anticipated that the color index calculated using linear interpolation would provide a reduction of the induced color index error in a situation where the two signatures are behaving smoothly (linearly). Whereas, it is anticipated that the linearly interpolated color index may result in a larger induced color index error when the two signatures are not behaving smoothly (non-linearly).

6.0 REFERENCES

[1] T. E. Payne, S. A. Gregory, F. J. Vrba and K. Luu, "Utility of a Multi-Color Photometric Database," in *Advanced Maui Optical and Space Surveillance Technologies (AMOS) Conference*, Wailea, 2005.

[2] T. E. Payne, S. A. Gregory, D. T. Hall, C. J. Wetterer, K. Luu and F. Vrba, "SSA Analysis of GEOS Photometric Signature Classifications and Solar Panel Offsets," in *Advanced Maui Optical and Space Surveillance Technologies (AMOS) Conference*, Wailea, 2006.

[3] T. E. Payne, S. A. Gregory, J. Tombasco and L. Durr, "Satellite Monitoring, Change Detection, and Characterization Using Non-Resolved Electro-Optical Data From a Small Aperture Telescope," in *Advanced Maui Optical and Space Surveillance Technologies (AMOS) Conference*, 2007.

[4] T. E. Payne, P. J. Castro, J. W. Moody, E. A. Beecher, N. D. Fisher and R. I. Acosta, "A Discrimination Analysis of Sloan and Johnson Photometric Systems for Non-Resolved Object Characterization," in *Advanced Maui Optical and Space Surveillance Technologies (AMOS) Conference*, 2016.

[5] P. Dao, K. Weasenforth, J. Hollon, T. E. Payne, K. Kinateder and A. Kruchten, "Machine Learning-based Stability Assessment and Change Detection for Geosynchronous Satellites," in *Advanced Maui Optical and Space Surveillance Technologies (AMOS) Conference*, 2018.

7.0 ACKNOWLEDGEMENTS

The authors would like to acknowledge Dr. Andy Suzuki (BlueHalo) for supporting the collection of the observations data used for the analysis in this paper.